

## RESEARCH ARTICLE

# Revisiting the identification of canonical splice isoforms through integration of functional genomics and proteomics evidence

Hong-Dong Li<sup>1</sup>, Rajasree Menon<sup>1</sup>, Gilbert S. Omenn<sup>1,2,3</sup> and Yuanfang Guan<sup>1,2,4</sup>

<sup>1</sup> Department of Computational Medicine and Bioinformatics, University of Michigan, Ann Arbor, MI, USA

<sup>2</sup> Department of Internal Medicine, University of Michigan, Ann Arbor, MI, USA

<sup>3</sup> Department of Human Genetics, School of Public Health, University of Michigan, Ann Arbor, MI, USA

<sup>4</sup> Department of Electrical Engineering and Computer Science, University of Michigan, Ann Arbor, MI, USA

Canonical isoforms in different databases have been defined as the most prevalent, most conserved, most expressed, longest, or the one with the clearest description of domains or post-translational modifications. In this article, we revisit these definitions of canonical isoforms based on functional genomics and proteomics evidence, focusing on mouse data. We report a novel functional relationship network-based approach for identifying the highest connected isoforms (HCIs). We show that 46% of these HCIs are not the longest transcripts. In addition, this approach revealed many genes that have more than one highly connected isoforms. Averaged across 175 RNA-seq datasets covering diverse tissues and conditions, 65% of the HCIs show higher expression levels than nonhighest connected isoforms at the transcript level. At the protein level, these HCIs highly overlap with the expressed splice variants, based on proteomic data from eight different normal tissues. These results suggest that a more confident definition of canonical isoforms can be made through integration of multiple lines of evidence, including HCIs defined by biological processes and pathways, expression prevalence at the transcript level, and relative or absolute abundance at the protein level. This integrative proteogenomics approach can successfully identify principal isoforms that are responsible for the canonical functions of genes.

Received: April 28, 2014  
Revised: August 11, 2014  
Accepted: September 23, 2014

**Keywords:**

Alternative splicing / Canonical isoforms / Highest connected isoforms / Integrative proteogenomics / Major transcripts



Additional supporting information may be found in the online version of this article at the publisher's web-site

## 1 Introduction

In mammalian systems, more than 90% of the multiexon genes are capable of producing multiple transcripts by alternative splicing (AS) [1, 2], which may carry out similar,

different, or even opposite biological functions [1–14]. The resulting splice variants greatly increase the repertoire of gene products and therefore their functional complexity. To interrogate the main functions of these gene products, significant efforts have been devoted to identifying the canonical, major or principal isoform of each gene [15–18]. However, the definition of canonical isoforms is complex and different in different databases. For example, UniProt defines the canonical isoforms as the most prevalent, most conserved,

**Correspondence:** Dr. Yuanfang Guan, Department of Computational Medicine and Bioinformatics, University of Michigan, 2044 Palmer Commons, Ann Arbor, MI, USA

**E-mail:** gyuanfan@umich.edu

**Abbreviations:** **AFR**, average functional relationship; **AS**, alternative splicing; **HCIs**, highest connected isoforms; **NCl**s, nonhighest connected isoforms

\*Additional corresponding author: Gilbert S. Omenn, Department of Computational Medicine and Bioinformatics, University of Michigan, Ann Arbor, MI, USA  
E-mail: gomenn@med.umich.edu

longest, or the one with clear description of domains or posttranslational modifications (<http://www.uniprot.org/faq/30>). UCSC designates the longest splice variant of a gene as the canonical isoform (<http://genome.ucsc.edu/cgi-bin/hgTrackUi?db=hg19&g=knownGene>). Rodriguez et al. defined the principal or canonical isoforms as the most conserved transcripts across related species and the ones that specify functional units in their sequences [16]. Finally, the “major” transcripts have been defined by their relatively high expression level in multiple studies [17, 18], despite the complex regulation of AS [10, 19, 20] most genes express one major transcript based on genome-scale expression data in human and mouse [15–18]. Bahar et al. observed that there is a single dominant isoform per gene for 80% of genes based on full-length transcript or expression sequence tag data [15]. The ENCODE project [21] found that most genes express a major transcript at a relatively high level, even when several AS isoforms tend to be expressed simultaneously [17]. Similarly, González-Porta et al. revealed one dominant transcript per gene through transcriptome analysis of human tissues and cell lines and hypothesized that, although some minor transcripts may play a functional role in specific tissues, the major ones are likely to be the main contributors to the proteome [18]. One interesting finding in these studies [15, 16, 18] is that the expression-based or conservation-based principal isoforms share only a limited percentage of sequence (50–75%) with the longest isoforms, showing an inconsistency between these definitions.

The above disparate definitions of canonical isoforms (summarized in Supporting Information Table 1) call for an approach that integrates multiple lines of evidence to refine the identification of canonical isoforms, which more reliably reflect the main functions of the genes. Recent developments in proteogenomics approaches allow us to harness the wealth of information available at the proteome level and apply it to the available genomic and transcriptomic information [22]. Such a proteogenomics approach has been successfully used in annotating expression sequence tag databases [23], predicting novel genes [24–26], and correcting existing gene models [24]. Most relevant to this study, a proteogenomics approach can be used to correct or identify novel splice isoforms [22].

To address the challenge of identifying canonical isoforms, we report here a proteogenomics approach that integrates multiple levels of evidence, including functional relationship networks based on genomic data, transcriptomic RNA-seq data, and proteomic data. At the functional relationship network level, the highest connected isoforms (HCIs) are identified based on cofunctional connections with many other genes in the same biological pathways or processes. This network was built by integrating heterogeneous functional genomic data from RNA-seq, exon array, protein docking, and pseudoamino acid composition [27]. We performed a genome-scale analysis of the local isoform-level networks for 3427 validated multi-isoform mouse genes (based on RefSeq database v37.2), and identified the HCIs for each multi-isoform gene. At the transcript expression level, we found a

high level of overlap between the HCIs and relatively highly expressed splice variants. At the protein level, we identified the expressed isoforms to validate the canonical isoforms that were identified based on functional relationship networks and the transcriptomic data. We found significant overlap across the canonical isoforms identified through these three levels of analysis.

## 2 Materials and methods

### 2.1 The functional network approach for identifying canonical isoforms

Functional approaches have been shown to be promising in understanding for example gene functions, networks, and gene–disease relationships [28–32]. In this work, functional networks will be used to help identify canonical isoforms. The rationale in identifying canonical isoforms that are representative of their major gene functions is that they should be supported by multiple levels of functional genomics and proteomics evidence. The network-based approach anticipates that these isoforms participate in important biological pathways and processes, and therefore are expected to have more functional relationships with other transcripts/proteins. To analyze such functional relationships, we utilized the genome-wide functional relationship network at the isoform level for the mouse, which was generated through Bayesian network based multiple instance learning [27, 33–37]. This network integrates heterogeneous genomic data at the isoform level, encompassing 11 RNA-seq datasets (146 samples), 52 exon array datasets (1273 samples), 1 protein docking dataset, and 1 amino acid composition dataset. For each RNA-seq or exon array dataset, the correlation between isoforms was calculated to be used as an isoform pair feature; each score in the protein docking data represents how likely two protein isoforms are to bind each other; and the pseudoamino acid composition data reflect how similar two proteins are in terms of both percent composition and physiochemical properties of amino acids [27]. The algorithm is an iterative method, in which we used a Bayesian classifier. Briefly, each isoform pair can be represented by an  $n$ -dimensional feature vector  $(E_1, E_2, \dots, E_n)$ . With the Bayesian classifier, the probability that an isoform pair belonging to the positive class can be calculated using the following formula:

$$P(\gamma = 1 | E_1, E_2, \dots, E_n) = \frac{P(\gamma = 1) \prod_{i=1}^n P(E_i | \gamma = 1)}{C} \quad (1)$$

where  $P(\gamma = 1)$  is the prior probability for a sample (isoform pair) to be positive,  $P(E_i | \gamma = 1)$ ,  $i = 1, 2, \dots, n$ , is the probability of the  $i$ th feature given the observed value, conditioned that the isoform pair is functionally related and  $C$  is a constant normalization factor. The functionally related isoform pairs

are identified and used in the next iteration to train the model until convergence. In this network, each node represents an isoform, and the connection between two isoforms (of different genes) represents the probability ranging from 0 to 1 that two isoforms work in the same biological process/pathway.

To quantify the likelihood that each isoform is functionally related to other isoforms through participating the same biological process/pathway, we defined an average functional relationship (AFR) score, which is calculated as the average of the functional relationships between the isoform and its top connected neighbors (Fig. 1A). The AFR score in this work is calculated using a local network containing the top 25 functionally related neighbors, thereby avoiding weak and noisy functional connections. The probabilistic AFR score ranges from 0 to 1. Then, within each multi-isoform gene in the mouse (3427 validated in the RefSeq database, version 37.2), we calculated an AFR score for each of its isoforms and defined the one with the highest AFR score as the HCI of this gene. The remaining isoforms are treated as nonhighest connected isoforms (NCIs).

We expected that the AFR scores (representing how “highly connected” the isoforms are) would be quite different between HCI and corresponding NCIs for some genes, while for other genes these values are similar. To quantify such difference between isoforms of a multi-isoform gene, we calculated the ratio of the maximal to minimal AFR score of isoforms using the following formula:

$$r = AF R_{\max} / AF R_{\min} \quad (2)$$

In the above equation, a higher ratio  $r$  represents more difference between the “highly functionally connected” isoform and the relatively less functionally connected isoforms and vice versa.

## 2.2 Processing heterogeneous RNA-seq data

A total of 117 mouse RNA-seq datasets (containing 811 experiments) from the Sequence Read Archive database were initially downloaded on May 1, 2012. These data cover a wide range of experimental conditions and different tissues. For each experiment, TopHat (v2.0.051) [38, 39] was used to align the reads against the mouse reference genome (NCBI gene build, version 37.2). The expression levels of transcripts in terms of FPKM (fragments per kilobase of exon per million fragments) were estimated using Cufflinks (v2.0.0) [38]. For quality control, experiments with fewer than 10 million reads or covering less than 50% of the genes were removed. We finally obtained 41 datasets with 321 experiments with each dataset containing at least four experiments. Within each dataset, transcripts with missing values occurring in more than 50% experiments were removed for ensuring accurate expression value estimation. Of the 41, 11 RNA-seq datasets were used to build the functional relationship network at the splice isoform level for the mouse in our previous study [27].

The remaining 30 datasets were used as an independent test set for analyzing the expression behaviors of HCIs and NCIs in this study (Supporting Information File 1 for the full description of the RNA-seq datasets used, Supporting Information Fig. 1 for the number of expressed transcripts).

## 2.3 Proteomic data from eight normal tissues of mouse

The proteins expressed in eight normal mouse tissues were generated from publicly available data. Mass spectrometric mzXML files for breast (PAe000416), liver (PAe000297), and brain (PAe000359, PAe000370, PAe000373, and PAe000380) were downloaded from PeptideAtlas [40]. The mzXML files for the normal samples from these datasets were searched against our custom built ECgene database using X!Tandem software [41]; the search parameters used were the same as those of the original studies. The custom ECgene database was constructed by combining Ensembl and ECgene databases, as described previously [42]. Peptides identified with false discovery rate <1% were used to identify the proteins. The splice variant protein identifications were generated according to our published peptide to protein integration method [42]. The steps involved in the integration algorithm are as follows:

- (1) Peptides (false discovery rate <1%) are ordered by the number of spectra matching each peptide.
- (2) The peptide with the largest number of matching spectra is selected.
- (3) Proteins containing this peptide were ranked by decreasing number of total distinct peptides identified, decreasing number of total spectra, increasing expect value, and then increasing protein length.
- (4) The highest ranking protein was selected to be included in the final integrated protein list; if a tie exists, preference was given to an Ensembl protein over an ECgene protein.
- (5) All other peptides contained within this protein were removed from the peptide list.
- (6) Steps 3–5 were repeated until no peptides remain in the peptide list.

Only the splice variant proteins identified from the normal tissue samples were used for this study.

*Breast:* Whiteaker et al. [43] performed LC-MS/MS of tumor and normal mammary tissues from a conditional HER2/neu-driven mouse model of breast cancer. The original study reported that cancerous and normal tissues were harvested from five doxycycline-inducible, MMTV-rtTA/TetO-NeuNT mice and five normal mice, respectively, and processed separately into tissue lysates. Two pools were prepared, containing equal mass of protein, and digested by trypsin for mass spectrometric analysis. This dataset was utilized by Menon and Omenn [44] in our early

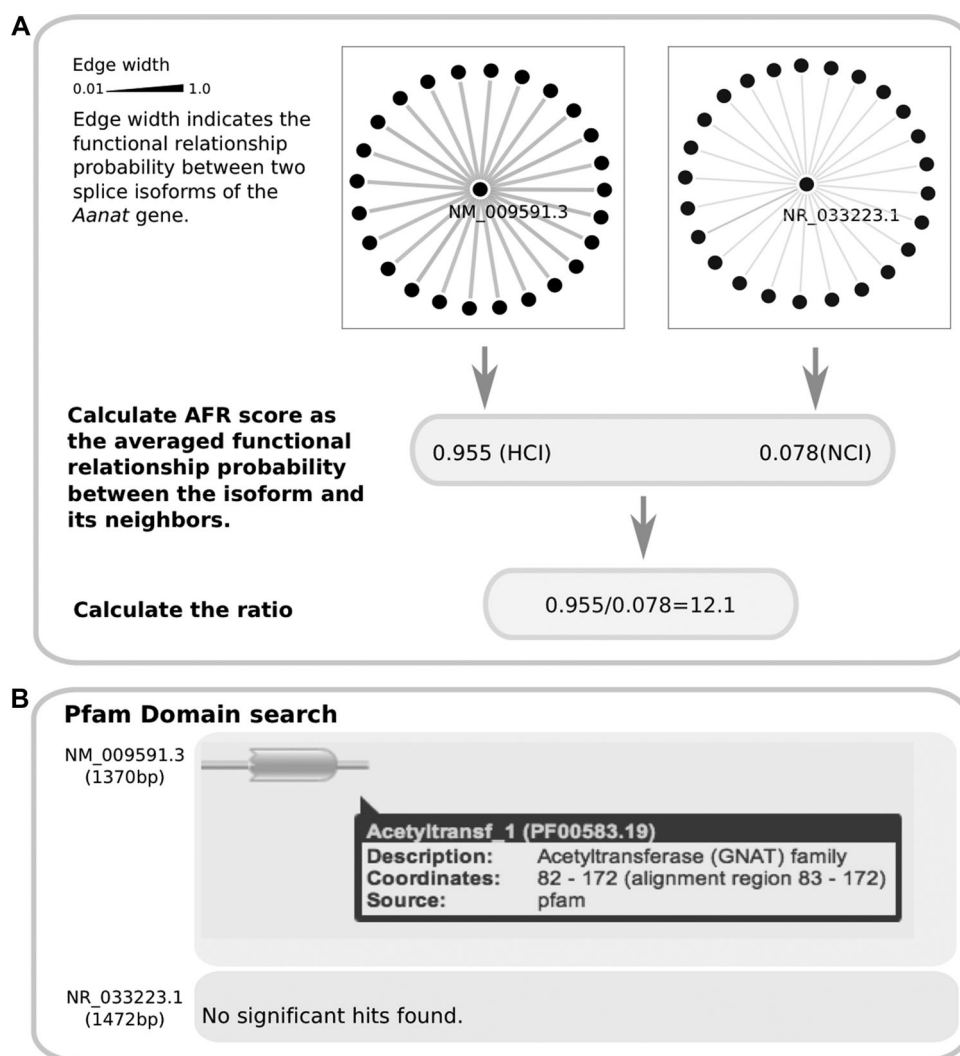


**Figure 1.** Illustration of how to identify HCI based on the functional relationship network, using the *Aanat* gene as an example. (A) In the functional relationship network, a single node represents an isoform and the connection between two isoforms represents the probability that they work in the same biological process or pathway. The edge width represents the functional relationship probability between two isoforms. The AFR score is calculated as the average connection of the top interactions for each isoform. The AFR of the two isoforms NM\_009591.3 and NR\_033223.1 of *Aanat* are 0.955 and 0.078, respectively. Therefore, NM\_009591.3 was selected as the HCI of *Aanat*. The ratio of the maximal AFR score to the minimal AFR score of each gene was calculated. (B) Protein domain information based on Pfam for NM\_009591.3 and NR\_033223.1. NM\_009591.3, the shorter transcript, has an active acetyltransferase domain, while the longer transcript NR\_033223.1 has no domain identified.

studies of differential expression of splice isoforms in specific pathways in HER2/neu-driven breast cancers.

**Liver:** Shi et al. [45] reported a large-scale analysis of mouse liver tissue comprising a novel fractionation approach and high-accuracy MS techniques. Fractions enriched for soluble and membrane proteins from frozen tissue were separated by 1D electrophoresis followed by LC-MS/MS on the hybrid linear ion trap Orbitrap mass spectrometer (Thermo Fisher Scientific, Bremen, Germany).

**Brain:** The original study was conducted on mitochondrial, microsomal, cytoplasmic, and nuclear brain fractions using LCQ Deca XP MS (PAe000359, PAe000370, PAe000373, and PAe000380 at <http://www.peptideatlas.org/repository/>). A single list of distinct splice variants expressed in the brain was generated from the proteins identified from the mass spectrometric data analyses of all four brain fractions.

The splice variant proteins expressed in *adrenal*, *colon*, *eye*, *heart*, and *spleen* were extracted from the protein list pro-

vided in the supplementary material of a published study [46]. The original study used SILAC-labeled mice that were grown for more than two generations on a diet containing heavy lysine (Lys6–13C6) as their sole source of this amino acid, leading to complete labeling of their proteome [46]. Protein extracts from all SILAC-labeled tissues were combined to create a heavy spike-in protein standard; this standard was mixed with each of the unlabeled tissues in equal amounts [46]. LC-MS/MS measurements were performed on an Easy-nano-LC coupled to a linear ion trap Orbitrap XL mass spectrometer. The SILAC labeled to unlabeled ratio values were used for relative comparison of the protein expression across the different tissues [46]. We extracted the proteins identified for adrenal, colon, eye, heart, and spleen tissues when the labeled to unlabeled ratio was more than zero; these five tissues were chosen among the 28 tissues investigated in the study, as there were at least three genes with more than one isoform expressed. The numbers of identified protein isoforms in the eight tissues were shown in Supporting Information Fig. 1.

For this study, we considered only the proteins whose parent genes are known to have multiple isoforms according to the NCBI-validated isoform annotations.

### 3 Results

#### 3.1 Identify the HCIs in the mouse based on functional relationships

In the functional relationship network, a node represents an isoform, and the edge between nodes represents the probability (ranging from 0 to 1) that two isoforms work in the same biological process or pathway based on integrating heterogeneous experimental evidence. For each individual isoform of a multi-isoform gene, all of its functional connections are sorted in decreasing order first. Then, we calculated an AFR score as the average of the functional connection between the isoform and its top connected neighbors (Fig. 1A). The reason that we chose only the top connected isoforms is to avoid noisy connections and enable easy network visualization. AFR is used to describe the likelihood that an isoform would be functionally related to others. Taking the arylalkylamine *N*-acetyltransferase gene *Aanat* as an example, the AFR score of its isoform NM\_009591.3 is 0.955. The functional connections of this isoform are much stronger than those of the other isoform NR\_033223.1 (AFR = 0.078). NM\_009591.3 is therefore selected as the HCI of *Aanat* (Fig. 1A). Consistent with the predictions, NM\_009591.3 is a protein-coding transcript containing a functional acetyltransferase domain (Fig. 1B), whereas NR\_033223.1 is a noncoding transcript containing a 5'-most translational start codon, which renders it a candidate target for the nonsense-mediated decay pathway based on the NCBI gene database, directly supporting the prediction that NM\_009591.3 cannot be functionally highly connected to other proteins.

We identified the functionally HCIs for the 3427 multi-isoform genes based on the RefSeq gene annotation of mouse, resulting in 3427 HCIs and 5334 NCIs (Supporting Information File 2). So far, the functions of the splice isoforms are mainly inferred through computational prediction [35], instead of experimental validation. To our knowledge, isoform-specific functions are known only for a limited number of genes, which can be found in a recent review [37]. Among the 3427 HCIs, 165 are noncoding RNAs, of which most are from validated or predicted noncoding genes except for six genes (*Wac*, *Rai12*, *Zfp672*, *Ng23*, *4930583H14RIK*, and *Prr18*), which is consistent with our expectation that most coding gene functions are carried out by protein-coding transcripts and noncoding gene functions by noncoding transcripts.

There are cases in which the AFR scores of NCIs of genes are very close to that of the HCI; such NCIs could also be considered as highly connected isoforms. To cover such isoforms, we included them as HCI candidates if their AFR scores were 80% or more than that of the HCI (Supporting

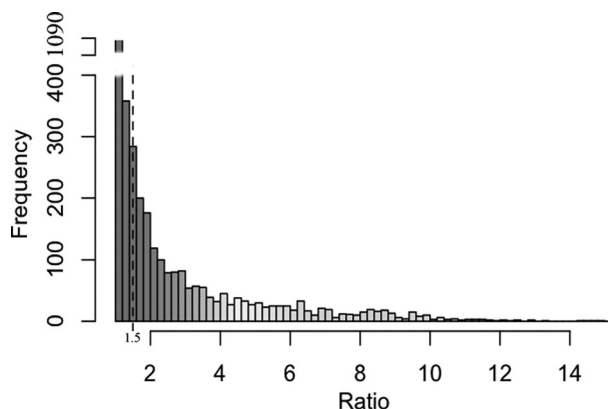


**Figure 2.** The distribution of the ratio of AFR scores between the most “functional” isoform and the least “functional” one (calculated using Formula 2) of all the 3427 multi-isoform genes of the mouse; 1829 of the 3427 genes have a ratio >1.5, implying the diversity of functional relationship between isoforms of the same gene. The ratio values range from 1.000 to 15.226.

Information File 3), which gives in total 2104 HCI candidates. When this threshold was set to 85 and 95%, the numbers of HCI candidates were 1394 and 942, respectively. As an example, the isoform NM\_013472.4 (AFR = 0.484) of *Anxa6* gene is the HCI, and the isoform NM\_001110211.1 (AFR = 0.426) is its HCI candidate.

We further calculated the ratio of AFR values of the most “functionally connected” isoform to the least “functionally connected” one, using formula (2), for each multi-isoform gene to see how different the functional relationship between isoforms can be. The distribution of the fold change values is shown in Fig. 2; 1829 of the 3427 genes (53.4%) have a value >1.500, implying a high diversity of functional relationship for many of the multi-isoform genes under study. The rest of the genes (46.6%) have an *r* ratio less than 1.500, likely implying that all isoforms of the gene carry out important functions and caution should be taken to assign canonical functional isoforms for these genes. For those genes having three or more isoforms, we also calculated the ratio of its highest AFR score to the second highest score to see how close the AFR scores of top connected isoforms can be. The distribution of this ratio (ranging from 1.000 to 9.656) is shown in Supporting Information Fig. 2. Of the 1092 genes coding at least three isoforms, we found that about 1/3 of them show quite different AFR scores between their highest and second-HCIs (ratio >1.500).

#### 3.2 Comparison between the functionally HCIs, the longest isoforms, and the most conserved isoforms

Within the 3427 multi-isoform genes, we compared the HCIs to the longest transcript or protein, if translated. We found that 1833 HCIs (53.5%) are also the longest isoforms

**Table 1.** The number of HCIs shared with canonical isoforms (defined as the longest transcripts) and the principal isoforms in the APPRIS database (defined by sequence and conservation), respectively

Canonical isoforms		APPRIS principal isoforms	
Shared	By chance	Shared <sup>a)</sup>	By chance
1833 (53.5%, $p = 1.55 \times 10^{-16}$ )	1495 $\pm$ 23 (43.6% $\pm$ 0.6%)	1402 (75.7%, $p = 1.32 \times 10^{-30}$ )	1074 $\pm$ 25 (58.0% $\pm$ 1.3%)

a) Of the 3427 multi-isoform genes, 1853 genes have annotated APPRIS principal isoforms.

(Table 1). Although the overlap is significant compared to the number by chance ( $p = 1.55 \times 10^{-16}$ ), there is often a large discrepancy between the HCIs and the longest isoforms (46.5% are inconsistent), indicating that the canonical isoforms defined by sequence length alone may not correctly reflect the ones with most functional connections (for full list of comparison between functionally highly connected isoforms and the longest isoforms, see Supporting Information File 4). The likely reason for this difference between HCIs and the longest isoforms is that the HCIs are identified by functional data whereas the longest isoforms are selected purely by sequence. The HCI of *Aanat* is NM\_009591.3 (1370 bp), which is shorter than NR\_033223.1 (1472 bp), providing an example in which the HCI is not the longest (Fig. 1B).

We further compared the HCIs to the isoforms in the APPRIS database [16], which are mainly based on sequence conservation as well as protein structures. While 1853 of the 3427 multi-isoform genes have annotated APPRIS principal isoforms, 1402 are in common (75.7%,  $p = 1.32 \times 10^{-30}$ ; Table 1, Supporting Information File 5). This fraction of overlapping is much higher than the overlap between the HCIs and longest isoforms. This result is consistent with previous observations at the gene level that the highest functionally connected genes or genes with more interaction partners tend to be more likely to be conserved in sequence [47], presumably due to higher evolutionary pressure imposed on genes with more interactions [48].

### 3.3 The HCIs show consistently higher expression than other isoforms at the transcript level

We investigated the expression signature of the HCIs at the transcript level. We compared the expression level between HCIs and NCIs based on 175 RNA-seq samples (from Sequence Read Archive, see dataset list in Supporting Information File 1). At the threshold  $\log_2(\text{FPKM}) > -5$ , the averaged number of expressed genes of these samples are 16 744. These 175 samples were not used in predicting the isoform networks of the mouse [27] and therefore served as independent evidence. They cover a variety of cell types and tissues, including but not limited to embryonic stem cells, muscle, kidney, liver, and brain. For each RNA-seq sample, we calculated the average and distribution of expression levels of the HCIs and NCIs, respectively. The mean of expression values of HCIs and NCIs in each sample is shown

in Fig. 3A. Strikingly, we found that, regardless of different tissues/cell lines and experimental conditions, on average HCIs consistently show higher expression levels than NCIs (see Supporting Information File 6) across all the samples (Fig. 3), except for the ten samples of one RNA-seq dataset, SRP008508. A 3'-end sequencing technique was used for studying transcript expression in this atypical dataset, which was not able to differentiate alternatively spliced isoforms. We further computed the expression distributions of HCIs and NCIs by combining all the experiments (Fig. 3B). Although there is overlap between the expression levels of HCIs and NCIs, we found that the expression levels of HCIs are significantly higher than the NCIs ( $p < 1 \times 10^{-20}$ , two-sample *t*-test). These results indicate a strong correlation between the HCIs defined by pathways/biological processes and the major transcripts defined as the relatively highly expressed copy [17].

### 3.4 Refining canonical isoform identification using proteomic datasets from diverse tissues

To investigate the expression patterns of HCIs at the protein level, we collected eight sets of proteomic data covering liver, breast, brain, adrenal, colon, eye, heart, and spleen in the mouse. We identified highly confident isoforms expressed in each tissue by their unique peptide sequences according to the protocol described previously [41–43, 45, 46]. For multi-isoform genes, we then compared the expressed isoform in each tissue to the predicted HCIs. In total, we observed 323 genes, which have protein isoforms expressed. Of them, we found that the HCIs of 206 genes overlap with the expressed protein isoform in at least one tissue, which is significantly higher ( $p < 10 \times 10^{-6}$ ) than the number by chance ( $166 \pm 10$ ) cases. These results suggest the overall consistency between HCIs identified by pathways and biological processes and the major expressed isoforms at the proteomic level of different tissues. For these 206 genes, the average expression at the transcript level of HCIs is higher than that of NCIs (Fig. 3C), which is expected based on the findings in Section 3.3. This implies that HCI is a good indicator of expressed proteins at both the transcript and protein level, although the correlation between transcript and protein expression has been shown to be usually from 0.4 to 0.6 in previous studies [49, 50]. For these 206 genes, the network-based, transcript expression based, and proteomic data all identified the same isoform to be the

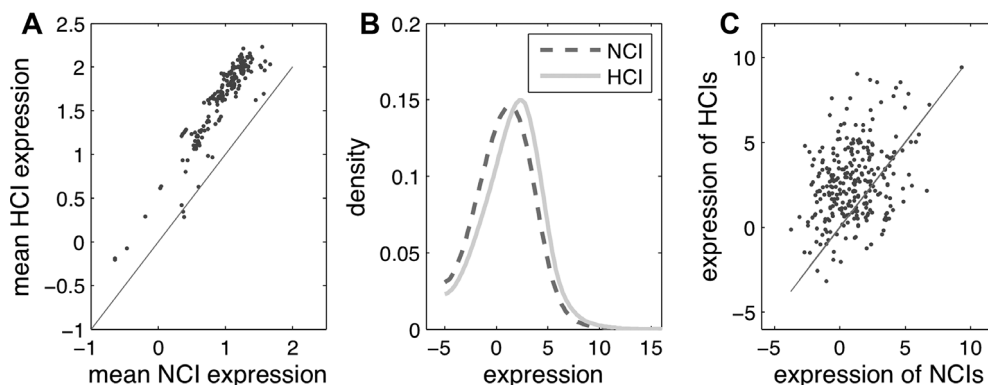


**Figure 3.** Comparison of expression levels between HCIs and NCIs. (A) For each of the 175 RNA-seq samples we collected from SRA, the mean expression was calculated for all HCIs and NCIs, respectively. Each dot represents the mean expression level of HCIs versus NCIs in one RNA-seq sample. (B) The distributions of expression levels of HCIs and NCIs calculated by combining all the 175 RNA-seq samples. (C) The expression values of HCIs against NCIs, averaged over the 175 RNA-seq samples, of which 206 genes have both transcript and protein level expression. Each dot represents a HCI–NCI pair within a gene (in total 277 pairs).

canonical isoform, making them strong cases where multiple lines of evidence support the identification of canonical isoforms.

For the other 117 (323–206) genes, their HCIs do not overlap with the expressed protein isoforms. Further, for these 117 genes, the average expression of HCIs at the transcript level is much higher than for NCIs ( $p < 5.9 \times 10^{-20}$ , Supporting Information Fig. 3). There are at least three reasons for this observation. First, for some genes, the AFR scores of their isoforms (such as the HCI candidate discussed in Section 3.1) are very close to that of HCI, indicating that these isoforms may actually be equally functional. Thus, it would be difficult to distinguish which isoform is the principal one. For example, the AFR scores of the two isoforms NM\_009295.2 and NM\_001113569.1 of the *Stxbp1* gene are 0.980 and 0.973, respectively. The protein isoform identified at the protein level was not the HCI (NM\_009295.2) but the other isoform (NM\_001113569.1). Another example is the *Ptbp1* gene whose two isoforms have similar scores, but its isoform with the lower AFR score (NM\_001077363.1) instead of the HCI NM\_008956.2, was also found in our proteomic data (described in Section 2.3). Second, compared to transcriptomic data, the number of proteins and protein isoforms that can be confidently identified in a proteomic experiment is smaller than for transcripts, with a lot of protein isoforms undetected. Third, we studied only eight tissues and the expression of certain isoforms can be tissue specific [51]. We listed 114 genes whose expressed proteins overlap with their HCIs and meanwhile have a ratio  $>1.500$  between the maximum and minimum AFR values (see Formula 2). Table 2 presents a list of isoforms with high confidence to be the canonical ones. This list represents the canonical isoforms supported by both participation in biological pathways and protein level expression. We observed that, for 35 of the 114 genes, their HCIs are expressed at the protein level in at least four tissues. For example, the HCIs of *Prosc* (proline synthetase cotranscribed) and *Tardbp* (TAR DNA binding protein) were observed in all the

eight tissues under study, which indicates that the biological role of these two proteins is carried out in diverse tissues by a single “functional” isoform. Other isoforms are only identified in some or one of the samples. These isoforms are either tissue specific in expression or their expression was not identified due to the limited coverage of proteomic sequences. An example of the former is *Syn3* (Synapsin III), which encodes a neuronal phosphoprotein and is brain specific (according to its GeneCards expression profile): its HCI NM\_013722.3 was found only in brain in our proteomic sample collection (Table 2).

## 4 Discussion

AS results in isoforms that greatly increase the repertoire of gene products and thus their functional complexity. To interrogate the main functions of these gene products, many studies have been devoted to identifying the canonical or principal isoforms. Previous criteria on the selection of such canonical isoforms are highly heterogeneous, based on sequence, conservation, expression, and existence of functional domains [15–18, 52]. However, they rarely consider whether the identified isoforms are indeed representative of the major function of the genes through analyzing their involvement in pathways and with proteomic evidence.

In this work, we used multiple lines of evidence integrating both functional genomic data and proteomic data to refine the identification of canonical isoforms. One important line of evidence we used was based on a functional relationship network, under the critical assumption that the functionally HCIs are more likely to represent the main functional gene product. We found that a large proportion of the HCIs are not the canonical isoforms as defined by the length of the transcripts. However, they do show strong overlap with the most conserved transcripts, the relatively highly expressed copies at the RNA level, and the identified splice copies at the

**Table 2.** The highest connected isoforms of 114 genes validated at the protein level using eight normal tissues of mouse<sup>a)</sup>

Gene	HCI	Tissue	Gene	HCI	Tissue
Aanat	NM_009591.3	LV	Snx7	NM_029655.3	AR, CL, SL
Cyp3a25	NM_019792.2	LV	Sbsn	NM_172205.3	AR, CL, EY, HT, SL
Mpp6	NM_019939.2	AR, CL, EY, HT, SL	Wdr33	NM_028866.3	BN
Psm2	NM_134101.2	LV, BN, AR, CL, EY, HT, SL	Mrps33	NM_010270.2	LV, AR
Mrpl15	NM_001177658.1	LV	Ahnak	NM_009643.1	LV, BT, AR, CL, EY, HT, SL
Tsr2	NM_001164578.1	AR, CL, HT	Lig1	NM_010715.2	AR, SL
Cstf3	NM_145529.3	LV	Sorbs1	NM_001034964.1	BN
Adhfe1	NM_175236.4	LV	Asb7	NM_080443.2	LV
Abca6	NM_147218.2	LV	Paccin3	NM_028733.3	AR, EY, HT
Ndufs6	NM_010888.2	LV	Plin1	NM_175640.2	BT
Hspa13	NM_030201.3	LV	Inadl	NM_172696.2	LV, CL, SL
Pex16	NM_145122.2	LV	Kctd14	NM_001012434.3	CL
Mrpl48	NM_198831.2	LV, AR, CL, EY, HT	Cyp2c50	NM_134144.2	LV
Wdr13	NM_026137.4	AR	Tmsb10	NM_025284.4	AR, CL, EY, SL
Prpsap2	NM_001164242.1	AR, CL, EY, HT, SL	Pick1	NM_008837.2	AR, CL
Aspn	NM_025711.3	AR, CL, EY, HT, SL	Hagh	NM_024284.2	AR, CL, EY, HT, SL
Adarb1	NM_130895.3	BN	Copg2	NM_017478.2–2	LV
Prosc	NM_054057.4	LV, BT, BN, AR, CL, EY, HT, SL	Syt7	NM_173068.2	AR, CL
Wtap	NM_001113533.1	CL	Fam134c	NM_026501.2	LV
Ociad1	NM_023429.4	LV	Ikzf1	NM_001025597.1	SL
Dars	NM_177445.5	LV, BN	Inpp4a	NM_030266.3	CL
Triobp	NM_001024716.1	AR, CL, EY, HT, SL	Setdb1	NM_001163641.1	SL
Dab1	NM_177259.3	LV	Aspscr1	NM_026877.2	LV
Lrp4	NM_172668.3	LV	Rab11fip1	NM_001080813.2	CL, SL
Gatad2a	NM_145596.3	AR, CL	Aamp	NM_146110.3	CL
Ripk3	NM_019955.2	CL, SL	Wdr61	NM_001025375.1	AR, CL, EY, HT, SL
Fbrsl1	NM_001142642.1	LV	Wasl	NM_028459.2	LV, AR, CL, EY, SL
Dlgap4	NM_001042487.1	AR, CL, EY, HT, SL	Ncam1	NM_001081445.1	BN
Brd1	NM_054054.2	LV	Brd4	NM_198094.2	LV
Tsc22d1	NM_207652.2	AR, CL, EY, HT, SL	Hnrnpa1	NM_001039129.3	AR, CL, EY, HT, SL
Nagk	NM_019542.2	AR, CL, EY, HT, SL	Egfr	NM_207655.2	LV
Jak2	NM_008413.2	CL	Ppih	NM_028677.4	AR, CL, EY, HT, SL
Mkl2	NM_001122667.2	AR, CL, SL	Dpp4	NM_010074.3	LV
Atp2a2	NM_001110140.3	LV	Thns1	NM_177588.2	AR, CL, EY, HT
Abhd11	NM_145215.2	LV	Tufm	NM_172745.3	BT
Hgd	NM_013547.3	LV	Dnajc6	NM_001164583.1	LV
Pex5l	NM_021483.3	AR, EY	Paccin2	NM_011862.3	AR, CL, EY, HT, SL
Nags	NM_145829.1	LV	Zfml	NM_008717.3	BN, CL, SL
Syn3	NM_013722.3	BN	Acdb6	NM_028250.3	LV
Ndr2	NM_001145959.1	BN	Bc030307	NM_001003910.2	LV
Copg	NM_017477.2	LV	Nfasc	NM_182716.4	BN
Dazap1	NM_001122605.1	AR, CL, EY, SL	Rrbp1	NM_024281.2	LV, BN
Golph3l	NM_146133.3	AR, CL, EY, HT, SL	Cd97	NM_011925.2	AR, CL, HT
Rlbp1	NM_020599.2	EY	Epb4.111	NM_001003815.2	AR, CL, EY, SL
Grk4	NM_019497.2	LV	Gngt2	NM_001038664.2	EY, SL
Brd2	NM_010238.3	AR, EY	Pabpc4	NM_130881.2	AR, CL, EY, HT, SL
Slc25a21	NM_172577.3	LV	Gimap4	NM_174990.3	AR, CL, EY, HT, SL
Bcap29	NM_001164090.1	AR	Eif2ak4	NM_013719.3	CL, SL
Glrx2	NM_001038592.1	LV	Pram1	NM_001002842.2	LV
Tardbp	NM_145556.4	LV, BT, BN, AR, CL, EY, HT, SL	Paccin1	NM_011861.2	AR, CL, EY, HT, SL
Rps24	NM_207634.1	LV	Erc1	NM_053204.2	LV, AR, CL, EY, HT, SL
Golga2	NM_133852.2	AR, CL, EY, HT, SL	Lmna	NM_001111102.1	AR, CL, EY, HT, SL
Tnpo2	NM_145390.4	AR, CL, EY, HT, SL	Rdx	NM_009041.3	AR, CL, EY, HT, SL
Acsc3	NM_001142804.1	LV	Ace2	NM_001130513.1	AR
Chchd6	NM_001167736.1	AR, CL, EY, HT	Acp1	NM_021330.4	AR, CL, HT, SL
2310035c23rik	NM_173187.3	AR, CL, EY, HT, SL	Pnkd	NM_025580.2	LV
Stk32c	NM_021302.3	BN	Eif4a2	NM_001123037.1	LV

a) Tissue abbreviation: LV, liver; BT, breast; BN, brain; AR, adrenal; CL, colon; EY, eye; HT, heart; SL, spleen. Only genes with the ratio of maximum to minimum AFR scores >1.5 are listed here.



protein level. These findings support the prediction for canonical isoforms by this integrative proteogenomic approach. On the other hand, our current findings may be limited by factors such as limited functional annotation data of splice isoforms, protein expression data used in our study, and the small number of proteomic experiments. Also, expression of transcripts and proteins are highly dynamic at different developmental stages of tissues or cell lines, which might add further complexity to the process of identifying canonical isoforms. It is expected that more reliable results would be obtained if more systematically processed proteomic data are available. Overall, the identified HCIs for the mouse provide an abundant source for investigating main functional products of 3427 multi-isoform genes; 206 of them are also further confirmed at the protein expression level. Our study adds a new aspect to the current knowledge on principal isoforms mainly based on sequence or conservation. We are building an analogous functional relationship network with human datasets.

This work is supported by NIH grants 1R21NS082212-01 (YG) and RM08029 and U54ES017885 (GSO).

The authors have declared no conflict of interest.

## 5 References

- [1] Pan, Q., Shai, O., Misquitta, C., Zhang, W. et al., Revealing global regulatory features of mammalian alternative splicing using a quantitative microarray platform. *Mol. Cell.* 2004, *16*, 929–941.
- [2] Pan, Q., Shai, O., Lee, L. J., Frey, B. J., Blencowe, B. J., Deep surveying of alternative splicing complexity in the human transcriptome by high-throughput sequencing. *Nat. Genet.* 2008, *40*, 1413–1415.
- [3] Matlin, A. J., Clark, F., Smith, C. W. J., Understanding alternative splicing: towards a cellular code. *Nat. Rev. Mol. Cell. Biol.* 2005, *6*, 386–398.
- [4] Gooding, C., Smith, C., Tropomyosin exons as models for alternative splicing. *Adv. Exp. Med. Biol.* 2008, *644*, 27–42.
- [5] Calarco, J. A., Saltzman, A. L., Ip, J. Y., Blencowe, B. J., Technologies for the global discovery and analysis of alternative splicing. *Adv. Exp. Med. Biol.* 2007, *623*, 64–84.
- [6] Mittendorf, K. F., Deatherage, C. L., Ohi, M. D., Sanders, C. R., Tailoring of membrane proteins by alternative splicing of pre-mRNA. *Biochemistry* 2012, *51*, 5541–5556.
- [7] Menon, R., Omenn, G. S., Proteomic characterization of novel alternative splice variant proteins in human epidermal growth factor receptor 2/neu-induced breast cancers. *Cancer Res.* 2010, *70*, 3440–3449.
- [8] Black, D. L., Mechanisms of alternative pre-messenger RNA splicing. *Annu. Rev. Biochem.* 2007, *72*, 291–336.
- [9] Wan, J., Masuda, T., Hackler, L., Torres, K. M. et al., Dynamic usage of alternative splicing exons during mouse retina development. *Nucleic Acids Res.* 2011, *39*, 7920–7930.
- [10] Barash, Y., Calarco, J. A., Gao, W., Pan, Q. et al., Deciphering the splicing code. *Nature* 2010, *465*, 53–59.
- [11] Tazi, J., Bakkour, N., Stamm, S., Alternative splicing and disease. *Biochim. Biophys. Acta* 2009, *1792*, 14–26.
- [12] Omenn, G. S., Yocum, A. K., Menon, R., Alternative splice variants, a new class of protein cancer biomarker candidates: findings in pancreatic cancer and breast cancer with systems biology implications. *Dis. Markers* 2010, *28*, 241–251.
- [13] Griffith, M., Griffith, O. L., Mwenifumbo, J., Goya, R. et al., Alternative expression analysis by RNA sequencing. *Nat. Methods* 2010, *7*, 843–847.
- [14] Emig, D., Salomonis, N., Baumbach, J., Lengauer, T. et al., AltAnalyze and DomainGraph: analyzing and visualizing exon expression data. *Nucleic Acids Res.* 2010, *38*, W755–762.
- [15] Bahar, T., Ben, S., Terry, G., Distribution of alternatively spliced transcript isoforms within human and mouse transcriptomes. *J. Omics Res.* 2011, *1*, 1–5.
- [16] Rodriguez, J. M., Maietta, P., Ezkurdia, I., Pietrelli, A. et al., AP-PRIS: annotation of principal and alternative splice isoforms. *Nucleic Acids Res.* 2013, *41*, D110–D117.
- [17] Djebali, S., Davis, C. A., Merkel, A., Dobin, A. et al., Landscape of transcription in human cells. *Nature* 2012, *489*, 101–108.
- [18] González-Porta, M., Frankish, A., Rung, J., Harrow, J., Brazma, A., Transcriptome analysis of human tissues and cell lines reveals one dominant transcript per gene. *Genome Biol.* 2013, *14*, R70.
- [19] Skotheim, R. I., Nees, M., Alternative splicing in cancer: noise, functional, or systematic? *Int. J. Biochem. Cell. Biol.* 2007, *39*, 1432–1449.
- [20] de Souza, J. E. S., Ramalho, R. F., Galante, P. A. F., Meyer, D., de Souza, S. J., Alternative splicing and genetic diversity: silencers are more frequently modified by SNVs associated with alternative exon/intron borders. *Nucleic Acids Res.* 2011, *39*, 4942–4948.
- [21] Dunham, I., Kundaje, A., Aldred, S. F., Collins, P. J. et al., An integrated encyclopedia of DNA elements in the human genome. *Nature* 2012, *489*, 57–74.
- [22] Renuse, S., Chaerkady, R., Pandey, A., Proteogenomics. *Proteomics* 2011, *11*, 620–630.
- [23] Pandey, A., Lewitter, F., Nucleotide sequence databases: a gold mine for biologists. *Trends Biochem. Sci.* 1999, *24*, 276–280.
- [24] Kalume, D., Peri, S., Reddy, R., Zhong, J. et al., Genome annotation of *Anopheles gambiae* using mass spectrometry-derived data. *BMC Genomics* 2005, *6*, 128.
- [25] Xia, D., Sanderson, S., Jones, A., Prieto, J. et al., The proteome of *Toxoplasma gondii*: integration with the genome provides novel insights into gene expression and annotation. *Genome Biol.* 2008, *9*, R116.
- [26] Castellana, N. E., Payne, S. H., Shen, Z., Stanke, M. et al., Discovery and revision of Arabidopsis genes by proteogenomics. *Proc. Natl. Acad. Sci. U S A* 2008, *105*, 21034–21038.
- [27] Li, H.-D., Menon, R., Eksi, R., Guerler, A. et al., Modeling the functional relationship network at the splice isoform level through heterogeneous data integration. *bioRxiv* 2013. doi:10.1101/001719.

- [28] Park, C. Y., Wong, A. K., Greene, C. S., Rowland, J. et al., Functional knowledge transfer for high-accuracy prediction of under-studied biological processes. *PLoS Comput. Biol.* 2013, *9*, e1002957.
- [29] Guan, Y., Ackert-Bicknell, C. L., Kell, B., Troyanskaya, O. G., Hibbs, M. A., Functional genomics complements quantitative genetics in identifying disease-gene associations. *PLoS Comput. Biol.* 2010, *6*, e1000991.
- [30] Guan, Y., Myers, C. L., Lu, R., Lemischka, I. R. et al., A genomewide functional network for the laboratory mouse. *PLoS Comput. Biol.* 2008, *4*, e1000165.
- [31] Wong, A. K., Park, C. Y., Greene, C. S., Bongo, L. A. et al., IMP: a multi-species functional genomics portal for integration, visualization and prediction of protein functions and networks. *Nucleic Acids Res.* 2012, *40*, W484–W490.
- [32] Guan, Y., Gorenshteyn, D., Schimenti, J. C., Handel, M. A. et al., Tissue-specific functional networks for prioritizing phenotypes and disease genes. *PLoS Comput. Biol.* 2012, *8*, e1002694.
- [33] Andrews, S., Tsochantaridis, I., Hofmann, T., Support vector machines for multiple-instance learning. *Advances Neural Information Processing Systems* 15. 2003.
- [34] Maron, O., Lozano-Perez, T., *Advances in Neural Information Processing Systems* 10. 1998, pp. 570–576.
- [35] Eksi, R., Li, H.-D., Menon, R., Wen, Y. et al., Systematically differentiating functions for alternatively spliced isoforms through integrating RNA-seq data. *PLoS Comput. Biol.* 2013, *9*, e1003314.
- [36] Li, H.-D., Menon, R., Omenn, G., Guan, Y., The emerging era of genomic data integration for analyzing splice isoform functions. *Trends Genet.* 2014, *30*, 340–347.
- [37] Omenn, G. S., Guan, Y., Menon, R., A new class of protein cancer biomarker candidates: differentially expressed splice variants of ERBB2 (HER2/neu) and ERBB1 (EGFR) in breast cancer cell lines. *J. Proteomics* 2014, *107*, 103–112.
- [38] Trapnell, C., Roberts, A., Goff, L., Pertea, G. et al., Differential gene and transcript expression analysis of RNA-seq experiments with TopHat and Cufflinks. *Nat. Protoc.* 2012, *7*, 562–578.
- [39] Trapnell, C., Pachter, L., Salzberg, S. L., TopHat: discovering splice junctions with RNA-Seq. *Bioinformatics* 2009, *25*, 1105–1111.
- [40] Desiere, F., Deutsch, E. W., King, N. L., Nesvizhskii, A. I. et al., The PeptideAtlas project. *Nucleic Acid Res.* 2006, *34*, D655–D658.
- [41] Craig, R., Beavis, R. C., TANDEM: matching proteins with tandem mass spectra. *Bioinformatics* 2004, *20*, 1466–1467.
- [42] Menon, R., Zhang, Q., Zhang, Y., Fermin, D. et al., Identification of novel alternative splice isoforms of circulating proteins in a mouse model of human pancreatic cancer. *Cancer Res.* 2009, *69*, 300–309.
- [43] Whiteaker, J. R., Zhang, H., Zhao, L., Wang, P. et al., Integrated pipeline for mass spectrometry-based discovery and confirmation of biomarkers demonstrated in a mouse model of breast cancer. *J. Proteome Res.* 2007, *6*, 3962–3975.
- [44] Menon, R., Roy, A., Mukherjee, S., Belkin, S. et al., Functional implications of structural predictions for alternative splice proteins expressed in Her2/neu-induced breast cancers. *J. Proteome Res.* 2011, *10*, 5503–5511.
- [45] Shi, R., Kumar, C., Zougman, A., Zhang, Y. et al., Analysis of the mouse liver proteome using advanced mass spectrometry. *J. Proteome Res.* 2007, *6*, 2963–2972.
- [46] Geiger, T., Velic, A., Macek, B., Lundberg, E. et al., Initial quantitative proteomic map of 28 mouse tissues using the SILAC mouse. *Mol. Cell. Proteomics* 2013, *12*, 1709–1722.
- [47] Mackay, T. F. C., Epistasis and quantitative traits: using model organisms to study gene-gene interactions. *Nat. Rev. Genet.* 2014, *15*, 22–33.
- [48] Park, S., Lehner, B., Epigenetic epistatic interactions constrain the evolution of gene expression. *Mol. Syst. Biol.* 2013, *9*, 645.
- [49] Guo, Y., Xiao, P., Lei, S., Deng, F. et al., How is mRNA expression predictive for protein expression? A correlation study on human circulating monocytes. *Acta Biochim Biophys Sin* 2008, *40*, 426–436.
- [50] Gry, M., Rimini, R., Stromberg, S., Asplund, A. et al., Correlations between RNA and protein expression profiles in 23 human cell lines. *BMC Genomics* 2009, *10*, 365.
- [51] Ellis, J. D., Barrios-Rodiles, M., Çolak, R., Irimia, M. et al., Tissue-specific alternative splicing remodels protein-protein interaction networks. *Mol. Cell* 2012, *46*, 884–892.
- [52] Tress, M. L., Wesselink, J.-J., Frankish, A., López, G. et al., Determination and validation of principal gene products. *Bioinformatics* 2008, *24*, 11–17.